Modeling Bubble and Drop Formation in Flowing Liquids in Microgravity

Ieehwan Kim, Yasuhiro Kamotani, and Simon Ostrach
Dept. of Mechanical and Aerospace Engineering, Case Western Reserve University, Cleveland, OH 44106

A theoretical model for the process of bubble and drop formation in flowing liquids, applicable for both terrestrial and microgravity environments, has been developed by using a force balance. The contact angle variation at the nozzle due to the bubble motion and the added mass coefficient of the bubble moving through a pipe have been theoretically analyzed, considering bubble motions during its expansion and detachment stages. Predictions of bubble size of the model show satisfactory agreement with available experimental results in the case of normal gravity. The effects of the nondimensional variables on bubble and drop size are evaluated in microgravity conditions. In microgravity, the bubble is detached from the nozzle only by the liquid flow drag, and in the region of low liquid velocity the bubble size becomes much larger than that in normal gravity.

Introduction

The power demands of spacecraft are expected to grow as high as one megawatt within the next 20 years (Mahefkey, 1982). The high operating power levels for future space applications require more efficient thermal transport techniques. Eastman et al. (1984) proposed the replacement of conventional single-phase flow systems with two-phase flow systems to obtain more effective thermal transport in space. Two-phase systems including gas/liquid and liquid/liquid contacting systems are common phenomena encountered in space applications, such as propulsion systems, power generation systems, cryogenic transfer and storage systems, life support systems, and other chemical/material process engineering systems. The design of two-phase systems for space applications requires a knowledge of heat- and mass-transfer processes under microgravity conditions. The distribution and size of the dispersed phase are very essential for the analysis of heat and mass transfer, pressure drop and flow pattern in two-phase systems. Therefore, there is a great need to study how the bubble size and frequency can be controlled in microgravity.

Under microgravity conditions, the body force becomes negligible and surface tension effects become more important, thus very large and more spherical bubble or drop formation is expected. For control of bubble size and frequency, an additional force is needed for detachment of the bubble or drop. One practical way to obtain this additional force is to use the drag force of a flowing liquid near a confined solid boundary (such as the wall of a pipe). Compared to research in the field of nucleate pool boiling under reduced-gravity conditions, the formation of bubbles and drops in flowing liquids does not appear to have been previously systematically studied, in spite of its potential importance in two-phase systems related to space applications.

There have been numerous experimental and theoretical studies of bubble and drop formation in a quiescent continuous phase in normal gravity. In spite of the fact that in most industrial equipment applications, bubbles and drops are formed in the continuous phase moving past nozzles or orifices, the formation of bubbles and drops in a flowing continuous phase has received much less attention. Sullivan et al. (1964) investigated the effect on bubble size of the velocity of a liquid flowing past a horizontally submerged orifice. Chuang and Goldschmidt (1970) proposed a model for bubble formation in a coflowing liquid based on correlations using the tube diameter and bubble frequency. Kumar and Kuloor (1970) suggested that the reduction in bubble volume due to the continuous phase velocity is attributed to an extra upward drag force which adds to buoyancy. Clift et al. (1978) suggested that the additional drag of the continuous fluid causes earlier or later detachment according to whether the drag force assists or impedes detachment. Sada et al. (1978) reported a decrease

Correspondence concerning this article should be addressed to Y. Kamotani.

in bubble size formed in flowing liquid and developed an empirical correlation for bubble size. Itoh et al. (1980) investigated drop formation in a flow parallel and normal to a nozzle and obtained empirical correlations based on the experimental data. They found that the drop size is smaller for a flow normal to the nozzle than for a flow parallel to it. Tsuge et al. (1981, 1983) investigated the effect of the velocity of a horizontal liquid flow on the size of a bubble and extended their model for bubble formation in a quiescent liquid to consider the effect of a flowing liquid velocity. Al-Hayes and Winterton (1981a, b) measured bubble diameter at detachment into a flowing liquid in a tube and developed a modified surface tension force using the equilibrium contact angle. They also investigated the bubble growth in flowing liquids to study mass transfer to air bubbles adhering to the inside wall of a tube with supersaturated liquid flowing past them. Kawase and Ulbrecht (1981) developed an empirical model of the process when bubbles and drops are formed at a nozzle submerged vertically in a continuous phase flow by simulating the influence of the continuous phase flow by a virtual inclination of the nozzle. Räbiger and Vogelpohl (1982, 1983) proposed a model of bubble formation valid for the whole gas-flow rate in stagnant and flowing liquids. Ghosh and Ulbrecht (1989) developed a theoretical analysis for the process of bubble formation under the influence of an external drag imposed by a flowing polymer solution. However, all the empirical correlations developed in normal gravity cannot be applied directly to a microgravity environment by simply setting "g" equal to a low value.

Bubble and drop formation in flowing liquids is a three-dimensional, unsteady process involving a moving interface and a complex flow field. In this study, a theoretical model using a macroscopic force balance, applicable for both normal and microgravity conditions, is developed for the formation of bubbles and drops in a uniform flowing liquid normal to the nozzle by using nondimensional parameters. The predictions of this model are compared with available experimental results in case of normal gravity. The effects of the nondimensional variables on bubble size are evaluated under microgravity conditions.

Theoretical Development

A schematic diagram of bubble formation is shown in Figure 1. Liquid or gas is injected normal to a uniform liquid flow in a pipe to generate drops or bubbles. It is the basic configuration in many two-phase systems. The present model is based on a force balance for the bubble or drop (hereafter simply called bubble). Although the bubble is attached to the nozzle, its shape is assumed to be approximately spherical when analyzing the liquid flow around it.

Important forces in the formation of a bubble are as follows:

$$\text{Buoyancy force;}\quad F_B=\frac{\pi}{6}D_B^3(\rho_c-\rho_d)g \tag{1a}$$

which acts vertically upward.

Surface tension force at the nozzle;

$$F_S=\sigma\pi D_N f_n(\phi) \tag{1b}$$

where $f_n(\phi)$ represents the fact the bubble motion is not in the direction of the nozzle axis, as described below. The bubble is attached to the nozzle by this force and the direction of the force will be discussed later.

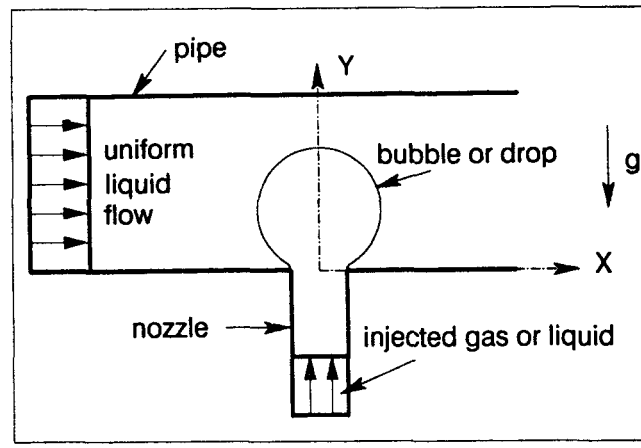

Figure 1. System for bubble and drop formation.

$$\text{Momentum flux;}\quad F_M=\rho_d\frac{Q_d^2}{\frac{\pi}{4}D_N^2} \tag{1c}$$

which is associated with the momentum of the injected fluid and acts in the injection direction.

$$\text{Inertia of bubble;}\quad F_I=\frac{d}{dt}\left(M\frac{ds}{dt}\right) \tag{1d}$$

which is associated with the momentum of the surrounding liquid motion induced by the bubble and opposes the bubble penetration.

$$\text{Liquid drag force;}\quad F_D=C_D\frac{1}{2}\rho_c U_{\text{eff}}^2 A_{\text{eff}} \tag{1e}$$

which acts in the downstream direction.

The bubble diameter at the instant of detachment will be found from a force balance at that moment:

$$\vec{F}_B+\vec{F}_M+\vec{F}_S+\vec{F}_D+\vec{F}_I=0 \tag{2}$$

Several analytical forms of a drag coefficient for bubbles and drops rising or freely falling through a continuous phase are available. In this study, the following correlations as well as the correlations for a solid sphere suggested by Bird et al. (1960) are used as the drag coefficient in Eq. 1e.

$$C_D=\frac{8}{Re_B}\left(\frac{2+3\bar{\mu}}{1+\bar{\mu}}\right)\quad\text{for}\quad Re_B\le 4\ \text{(Hadamard, 1911)} \tag{3a}$$

$$C_D=\frac{3.05(783\bar{\mu}^2+2{,}142\bar{\mu}+1{,}080)}{(60+29\bar{\mu})(4+3\bar{\mu})}Re_B^{-0.74}$$

$$\text{for } 4<Re_B\le 100\ \text{(Hamielec and Johnson, 1962)} \tag{3b}$$

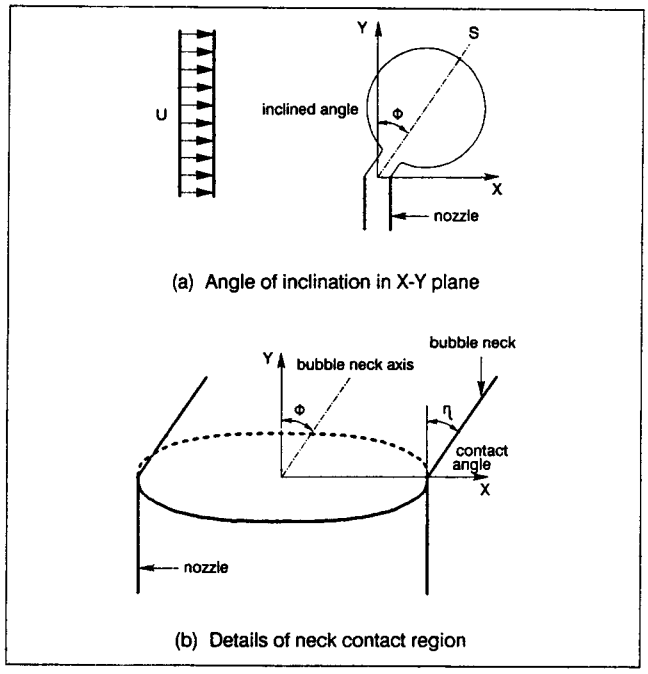

Figure 2. Variation of contact angle around the circumference of nozzle.

$$C_D = \frac{48}{Re_B}\left\{1 + \frac{3\mu}{2} + \frac{(2+3\overline{\mu})^2}{\sqrt{Re_B}}(B_1 + B_2 \ln Re_B)\right\}$$

for $100 < Re_B \leq 1{,}000$ (Clift et al., 1978) (3c)

where $Re_B = \rho_c U_{eff} D_B/\mu_c$ is the bubble Reynolds number, and B_1 and B_2 of Eq. 3c are functions of $\overline{\mu\rho}$ as given in Clift et al. (1978). In the bounded continuous phase in a pipe, the above drag coefficients would be changed by the wall effects. The wall boundary changes the boundary conditions of the external and internal flows and eventually changes the drag forces. Based on the empirical expression for the terminal velocity including the effect of the confining wall by Clift et al. (1978), Kim (1992) suggests the following correction of C_D for the wall effect,

$$C_{DW} = C_D \frac{1}{(1-\overline{D}_B^2)^3} \tag{4}$$

The added mass coefficient, which is needed in Eq. 1d, of the bubble either moving through an infinite continuous phase or expanding at a plate orifice is usually taken as 1/2 and 11/16, respectively. For a bubble moving through a bounded liquid in the pipe diameter of diameter D_P, the added mass is affected by the wall. In the Appendix, the added mass coefficients in that situation are derived based on potential flow theory.

Bubbles during growth are connected to the nozzle by a small neck. The bubble center moves normal to the liquid flow direction by the expansion process, as well as parallel due to the drag force of the flowing liquid. Thus, the bubble neck would be inclined with respect to the nozzle as shown in Figure 2. This fact was clearly observed in the experiments of Tsuge et al. (1981) and Ghosh and Ulbrecht (1989). The magnitude

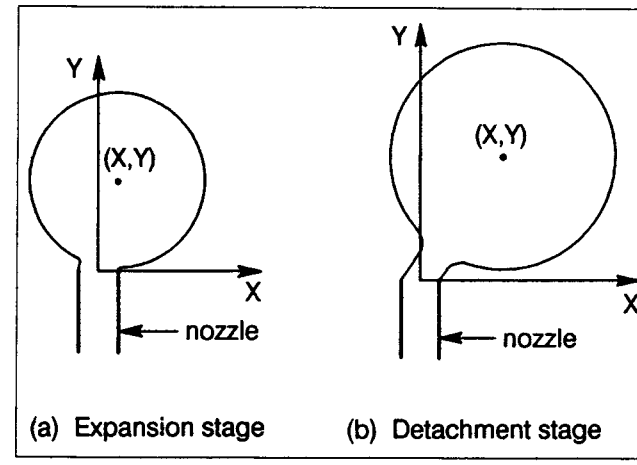

Figure 3. Expansion and detachment stages.

of the angle of inclination ϕ is taken to be the angle between Y axis and the line S connecting the nozzle center with the bubble center.

To calculate the surface tension force one has to know the contact angle (the angle between the Y axis and the bubble surface) at the nozzle. The contact angle (η) is not constant around the nozzle circumference. Referring to Figure 2b if one approximates the bubble neck shape as a circular cylinder with its axis in the ϕ direction, one gets

$$\eta = \phi \text{ at } \theta = 0,\ \pi \text{ and } \eta = 0 \text{ at } \theta = \pi/2,\ 3\pi/2$$

Based on that, it is assumed for simplicity that $\eta(\theta) = \phi(1 - 2\theta/\pi)$ in the range $0 \leq \theta \leq \pi/2$.

The surface tension force acts in the contact angle direction. Then, it can be easily shown that the X and Y components of the force are equal to $\sigma \sin \eta \cos \theta$ and $\sigma \cos \eta$, respectively, at a given θ. By integrating those components around the nozzle circumference the function $f_n(\phi)$ of Eq. 1b can be determined for the X and Y directions as follows:

$$f_{n,x}(\phi) = \cos\phi \frac{\phi}{\left(\frac{\pi}{2}\right)^2 - \phi^2}, \quad f_{n,y}(\phi) = \frac{\sin\phi}{\phi} \tag{5}$$

Equations of Motion

In this model, the bubble formation is assumed to take place in two stages, the expansion stage and the detachment stage, which was proposed by Kumar and Kuloor (1990) and agrees well with experimental data. During the expansion stage the bubble base remains attached to the nozzle tip (Figure 3a). The center of the bubble moves in the Y direction with a radial expansion velocity $(1/2)dD_B/dt$. Also, the center of the bubble is shifted to the X direction with a certain velocity dX/dt due to the drag force of the flowing liquid. At the beginning of the detachment stage, the upward force becomes greater than the downward force in the Y direction and the bubble base is lifted off from the nozzle (Figure 3b). During the detachment stage, the bubble is connected to the nozzle through a neck and the bubble center moves with a velocity dS/dt in the direction which is determined from the vector sum of the re-

sultant forces in X and Y direction until the neck is broken off.

Based on the basic fluid flow equations and the boundary conditions it can be shown that the following dimensionless parameters are important during the expansion and detachment stage.

$$Re_P=\rho_c U_{LS} D_P/\mu_c,\ We_P=\rho_c U_{LS}^2 D_P/\sigma,\ Fr=\rho_c U_{LS}^2/(\rho_c-\rho_d)gD_P$$
$$\overline{D}_B=D_B/D_P,\ \overline{D}_N=D_N/D_P,\ \overline{U}_{GS}=U_{GS}/U_{LS}$$
$$\overline{\rho}=\rho_d/\rho_c,\ \overline{\mu}=\mu_d/\mu_c,\ \overline{t}=t/(D_P/U_{LS})$$

where

$$U_{LS}=4Q_c/(\pi D_P^2),\ U_{GS}=4Q_d/(\pi D_P^2)$$

Then, the nondimensional bubble diameter at the instant of detachment can be expressed in the following general form:

$$\overline{D}_B=\overline{G}_n(We_P,\ Re_P,\ Fr,\ \overline{D}_N,\ \overline{U}_{GS},\ \overline{\rho},\ \overline{\mu}) \tag{6}$$

where the reference Froude number, Fr, becomes infinity under microgravity conditions. For typical gas-liquid and liquid-liquid systems, the maxima of $\overline{\rho}$ and $\overline{\mu}$ are approximately unity. The value of $\overline{D}_N$ should be less than unity in the present model. The range of Re_P and We_P are related to the dependability of the predictions of the present model based on the spherical shape assumption.

During the expansion stage, a set of force balance equations is needed for the X and Y directions. The component of surface tension in each direction can be obtained from Eqs. 1b and 5. The inertia masses in the X and Y directions are given by:

$$M_x=\frac{\pi}{6}D_B^3(\rho_d+C_{MX}\rho_c),\quad M_Y=\frac{\pi}{6}D_B^3(\rho_d+C_{MY}\rho_c) \tag{7}$$

The effective liquid velocities in the X and Y directions are:

$$U_{eff,x}=U_{LS}-\frac{dX}{dt},\quad U_{eff,y}=\frac{1}{2}\frac{dD_B}{dt} \tag{8}$$

And the effective projection area is $A_{eff}=\pi D_B^2/4$.

The nondimensional forms of important forces of Eq. 1 based on the reference force $F_R=\rho_c U_{LS} D_P^2$ are given by:

$$\overline{F}_B=\frac{\pi}{6}\frac{1}{Fr}\overline{D}_B^3,\quad \overline{F}_M=\frac{\pi}{4}\overline{\rho}\,\overline{U}_{GS}^2\frac{1}{\overline{D}_N^2}$$
$$\overline{F}_{S,X}=\frac{\pi}{We_P}\overline{D}_N\cos\phi\frac{\phi}{\left(\frac{\pi}{2}\right)^2-\phi^2},\quad \overline{F}_{S,Y}=\frac{\pi}{We_P}\overline{D}_N\sin\phi\frac{1}{\phi}$$
$$\overline{F}_{D,X}=C_{DW}\frac{1}{2}\overline{U}_{eff}\overline{U}_{eff,x}\overline{A}_{eff} \tag{9}$$
$$\overline{F}_{D,Y}=C_{DW}\frac{1}{2}\overline{U}_{eff}\overline{U}_{eff,y}\overline{A}_{eff}$$

$$\overline{F}_{I,X}=\frac{\pi}{12}\frac{dC_{MX}}{d\overline{D}_B}\overline{U}_{GS}\overline{D}_B\frac{d\overline{X}}{d\overline{t}}+\frac{\pi}{4}(C_{MX}+\overline{\rho})\overline{U}_{GS}\frac{d\overline{X}}{d\overline{t}}+\frac{\pi}{6}(C_{MX}+\overline{\rho})\overline{D}_B^3\frac{d^2\overline{X}}{d\overline{t}^2}$$
$$\overline{F}_{I,Y}=\frac{\pi}{48}\frac{dC_{MY}}{d\overline{D}_B}\overline{U}_{GS}^2\frac{1}{\overline{D}_B}+\frac{\pi}{48}(C_{MY}+\overline{\rho})\overline{U}_{GS}^2\frac{1}{\overline{D}_B^2}$$

where

$$\sin\phi=\frac{\overline{X}}{\left\{\overline{X}^2+\left(\frac{\overline{D}_B}{2}\right)^2\right\}^{1/2}},\quad \cos\phi=\frac{\frac{1}{2}\overline{D}_B}{\left\{\overline{X}^2+\left(\frac{\overline{D}_B}{2}\right)^2\right\}^{1/2}},$$
$$\overline{U}_{eff,x}=1-d\overline{X}/d\overline{t},\ U_{eff,y}=\overline{U}_{GS}/4\overline{D}_B^2,$$
$$\overline{U}_{eff}=\left\{\overline{U}_{eff,x}^2+\overline{U}_{eff,y}^2\right\}^{1/2}$$
$$\overline{A}_{eff}=\pi\overline{D}_B^2/4,\ \overline{X}=X/D_P,\ Re_B=Re_P\overline{U}_{eff}\overline{D}_B$$

The nondimensional form of Eq. 2 in the X direction then becomes:

$$\frac{\pi}{6}(C_{MX}+\overline{\rho})\overline{D}_B^3\frac{d^2\overline{X}}{d\overline{t}^2}+\frac{\pi}{12}\overline{U}_{GS}\left\{\frac{dC_{MX}}{d\overline{D}_B}\overline{D}_B+3(C_{MX}+\overline{\rho})\right\}\frac{d\overline{X}}{d\overline{t}}$$
$$=C_{DW}\frac{\pi}{8}\overline{D}_B^2\left\{\left(1-\frac{d\overline{X}}{d\overline{t}}\right)^2+\left(\frac{1}{4}\frac{\overline{U}_{GS}}{\overline{D}_B^2}\right)^2\right\}^{1/2}\left(1-\frac{d\overline{X}}{d\overline{t}}\right)-\frac{\pi}{We_P}\overline{D}_N\cos\phi\frac{\phi}{\left(\frac{\pi}{2}\right)^2-\phi^2} \tag{10}$$

The nondimensional form of Eq. 2 in the Y direction becomes:

$$\frac{\pi}{48}\overline{U}_{GS}^2\left\{\frac{dC_{MY}}{d\overline{D}_B}\frac{1}{\overline{D}_B}+(C_{MY}+\overline{\rho})\frac{1}{\overline{D}_B^2}\right\}=\frac{\pi}{6}\frac{1}{Fr}\overline{D}_B^3-\frac{\pi}{We_P}\overline{D}_N\sin\phi\frac{1}{\phi}+\frac{\pi}{4}\overline{\rho}\,\overline{U}_{GS}^2\frac{1}{\overline{D}_N^2}-C_{DW}\frac{\pi}{32}\overline{U}_{GS}\left\{\left(1-\frac{d\overline{X}}{d\overline{t}}\right)^2+\left(\frac{1}{4}\frac{U_{GS}}{\overline{D}_B^2}\right)^2\right\}^{1/2} \tag{11}$$

During the detachment stage, the inertia mass is approximately taken as:

$$M=\frac{\pi}{6}D_B^3\left\{\rho_d+\frac{1}{2}\rho_c(C_{MX}+C_{MY})\right\} \tag{12}$$

The nondimensional forms of the buoyancy force and the momentum flux of the dispersed phase are the same as those in Eq. 9. The nondimensional form of the surface tension force is the same as that in Eq. 9, but $\sin\phi$ and $\cos\phi$ in their expressions are given by:

$$\sin\phi=\overline{X}/(\overline{X}^2+\overline{Y}^2)^{1/2},\quad \cos\phi=\overline{Y}/(\overline{X}^2+\overline{Y}^2)^{1/2} \tag{13}$$

where $\bar{X}$ and $\bar{Y}$ is the bubble center position during the detachment stage.

The nondimensional forms of other forces are given by:

$$\bar{F}_{D,X}=C_{DW}\frac{1}{2}\bar{A}_{eff},\quad \bar{F}_{D,S}=C_{DW}\frac{1}{2}\left(\frac{d\bar{S}}{d\bar{t}}\right)^2\bar{A}_{eff}$$

$$\bar{F}_{I,S}=\frac{\pi}{24}\bar{U}_{GS}\left\{\frac{d(C_{MX}+C_{MY})}{d\bar{D}_B}\bar{D}_B+3(C_{MX}+C_{MY}+2\bar{\rho})\right\}\frac{d\bar{S}}{dt}+\frac{\pi}{12}(C_{MX}+C_{MY}+2\bar{\rho})\bar{D}_B^3\frac{d^2\bar{S}}{d^2\bar{t}} \quad (14)$$

where $\bar{S}=S/D_P$ and S is the bubble center position.

During the detachment stage, the nondimensional form of Eq. 2 becomes

$$\frac{\pi}{12}(C_{MX}+C_{MY}+2\bar{\rho})\bar{D}_B^3\frac{d^2\bar{S}}{d\bar{t}^2}+\frac{\pi}{24}\bar{U}_{GS}\left\{\frac{d(C_{MX}+C_{MY})}{d\bar{D}_B}\bar{D}_B+3(C_{MX}+C_{MY}+2\bar{\rho})\right\}\frac{d\bar{S}}{d\bar{t}}=\left[\left\{C_{DW}\frac{\pi}{8}\bar{D}_B^2-\frac{\pi}{We_P}D_N\cos\phi\frac{\phi}{\left(\frac{\pi}{2}\right)^2-\phi^2}\right\}^2+\left\{\frac{\pi}{6}\frac{1}{Fr}\bar{D}_B^3+\frac{\pi}{4}\bar{\rho}\bar{U}_{GS}^2\frac{1}{\bar{D}_N^2}-\frac{\pi}{We_P}\bar{D}_N\frac{\sin\phi}{\phi}\right\}^2\right]^{1/2}-C_{DW}\frac{\pi}{8}\bar{D}_B^2\left(\frac{d\bar{S}}{d\bar{t}}\right)^2 \quad (15)$$

As a detachment condition, two possible cases are considered (see Figure 4). For low liquid velocity, the bubble center would be moved in the X direction but would not be swept away. In this case, the bubble base is lifted off the nozzle at the end of the expansion stage and begins to rise vertically until the bubble neck breaks off (Figure 4a). For high liquid velocity, the bubble center would be severely shifted to the X direction and eventually be swept away from the nozzle even during the expansion stage (Figure 4b). In the former case, it is assumed the bubble will detach when the length of the bubble neck is equal to the nozzle diameter (Kumar and Kuloor, 1970). In the latter case, it is assumed the bubble will detach when the distance traveled by the bubble in the X direction is greater than or equal to the sum of the bubble radius and the nozzle radius (Kawase and Ulbrecht, 1981). Then, the nondimensional forms of the above two detachment conditions are given, respectively, by:

$$\bar{L}_N=(\bar{X}^2+\bar{Y}^2)^{1/2}-\frac{1}{2}\bar{D}_B\geq\bar{D}_N \quad (16a)$$

$$\bar{X}\geq\frac{1}{2}(\bar{D}_B+\bar{D}_N) \quad (16b)$$

During the bubble growth, the X direction force balance of

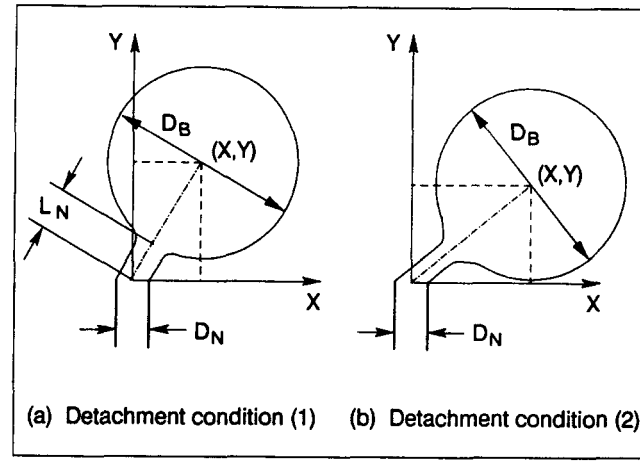

Figure 4. Detachment conditions of bubble.

Eq. 10 is computed by using the fourth-order Runge-Kutta method to determine the new position of bubble center in the X direction. The new position in the Y direction can be easily obtained from the simple expansion process. From this new position of bubble center, the angle of inclination ϕ is obtained and the force balance of Eq. 11 in the Y direction is checked. If the lefthand side is greater than the righthand side in Eq. 11, then the bubble is still in its expansion stage. This procedure is repeated by increasing $\bar{t}$ until either the force balance of Eq. 11 in the Y direction or the detachment condition of Eq. 16b is satisfied. If Eq. 16b is first satisfied, this means the bubble detaches during its expansion stage. Otherwise, the bubble goes into the detachment stage. During this detachment stage, Eq. 15 is solved to decide the new position of the bubble center and the detachment conditions are checked.

Bubble and drop formation in microgravity

As the Froude number in Eq. 6 approaches infinity in microgravity, the buoyancy force becomes negligible compared to other forces. The nondimensional bubble diameter at the instant of detachment is given by:

$$\bar{D}_B=\bar{H}_n(We_P, Re_P, \bar{D}_N, \bar{U}_{GS}, \bar{\rho}, \bar{\mu}) \quad (17)$$

With negligible buoyancy the bubble size tends to be large especially when the speed of the continuous phase is small. Therefore, one has to consider the limiting conditions when the bubble diameter becomes comparable with the pipe diameter. Consistent with the assumption made to facilitate the computation of the added mass, the limit of the bubble diameter is taken as the maximum diameter of a sphere within the square channel with the same cross-sectional area as the pipe of diameter D_P.

$$(\bar{D}_B)_{lim}=\sqrt{\pi}/2 \quad (18)$$

For large bubbles, the size of which approaches that of the pipe diameter, it was speculated by Dukler et al. (1988) that the average void fraction ϵ ranges from 0.4 to 0.5. In the present study, 0.45 is taken as the value of void fraction, ϵ, applicable

for the single bubble formation within a pipe. Then, the maximum nondimensional superficial gas velocity becomes:

$$(U_{GS})_{max} = 0.818 \tag{19}$$

If the bubble does not detach until its size reaches the limit of Eq. 18, it is speculated that the bubble would take the form of a large Taylor bubble the length of which is greater than the pipe diameter, but the analysis of this Taylor bubble is beyond the present model. It is known that deformation from the spherical shape for bubbles and drops rising or falling freely in systems of practical importance occur for $Re_B \geq 600$ from the result of Grace et al. (1976). Also, to satisfy the spherical shape assumption, the dynamic pressure of the flowing liquid should be less than the surface tension pressure at the interface of bubbles or drops. Then the maximum bubble Weber number should be approximately less than 8. The approximated maximum Re_B and We_B are taken as 600 and 3, respectively, to assure the assumption of spherical shape. In terms of Re_P and We_P the maximum values are taken to be as follows in the present analysis.

$$(Re_P)_{max} = 1{,}200, \quad (We_P)_{max} = 12$$

Results and Discussion

Comparison with experimental results in normal gravity

To test the predictive capability of our model, we have compared the drop size computed using the present model with the experimental data taken by Itoh et al. (1980). We computed the drop sizes for various experimental conditions, and it was found that the predictions agreed well with the data if the drag coefficient for a solid sphere was used (Kim et al., 1992). The fact that the internal circulation in the drop does not reduce drag as predicted by the various models for C_D is mainly because the fluid motion due to injection overwhelms the flow induced by the surrounding liquid in the liquid-liquid system used by Itoh et al.

Itoh et al. (1980) and Kawase and Ulbrecht (1981) obtained empirical equations for any fluid combination for drop size prediction based on the experimental data by Itoh et al. Both correlations contain two adjustable constants which were determined from the data. The experiment by Itoh et al. was conducted in a large container, so the important parameters are We_P, Fr, $\bar{\rho}$, $\bar{\mu}$ according to Eq. 6. The effect of Fr and $\bar{\rho}$ is considered to be negligible in the liquid-liquid experiment, so We_P and $\bar{\mu}$ are two parameters. However, Itoh et al. tried to correlate the data by the Weber number alone despite the fact that $\bar{\mu}$ varied by a factor of 6 in the experiments. Consequently, the data shows a noticeable scatter around the correlation curve.

Figure 5 shows the comparison of the predictions of our model using the drag coefficient for a solid sphere with Itoh's and Kawase and Ulbrecht's correlations for the specific continuous and dispersed phase fluids. In the region of low and high continuous phase velocities, the results of our model match well with both correlations. In the region of intermediate continuous phase velocity, the prediction of our model is larger or smaller than those values correlated by Itoh et al. and Kawase and Ulbrecht. Our model as well as their correlations show a reduction of drop diameter with increase of the continuous phase velocity beyond a certain value. Our results show that this reduction is related to the change of the detachment condition from Eqs. 16a to 16b. The specific continuous phase velocity at which this reduction starts is higher in our model than Itoh's and Kawase's correlations. This discrepancy is believed to be due to the nonspherical bubble shape in the experiment.

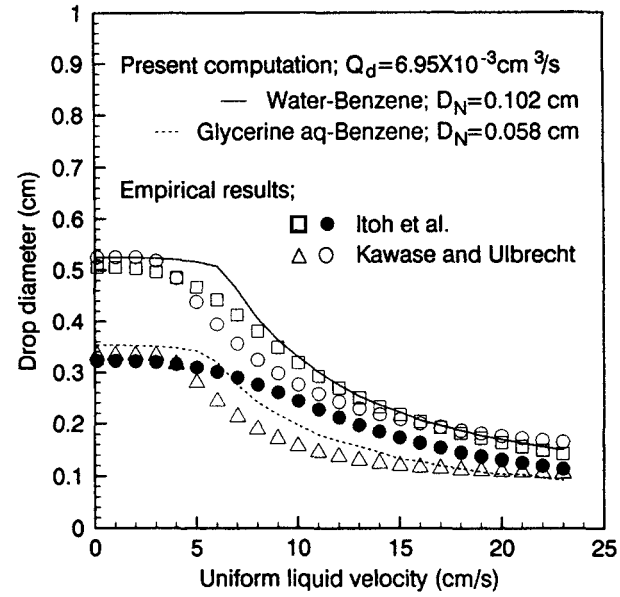

Figure 5. Comparison of present predictions with experimental correlations.

There are still some discrepancies between Itoh's and Kawase's correlations as seen in Figure 5, even though they used the same set of experimental data and contain two adjustable parameters. Considering that our model does not include any adjustable parameter and provides good agreement with the experimental results, the prediction of our model is satisfactory for the estimation of the bubble and drop size in a flowing liquid system.

Bubble and drop formation in microgravity

Our model is applied to an air-liquid system to estimate the bubble size for various conditions in microgravity. The effects of the nondimensional parameters and the reference variables on the bubble size are examined. Figure 6 shows the variation of nondimensional bubble diameter, $\overline{D}_B$, in an air-water system. The bubble tends to occupy a large portion of the pipe diameter and in some cases it becomes nearly as large as the pipe diameter (limiting $\overline{D}_B$ given by Eq. 18). Generally, $\overline{D}_B$, decreases with increasing reference Weber number, We_P, and with decreasing reference Reynolds number, Re_P. For fixed Re_P and We_P, $\overline{D}_B$ increases with increasing nondimensional superficial gas velocity, $\overline{U}_{GS}$, and with increasing nondimensional nozzle diameter, $\overline{D}_N$. Figure 6a shows $\overline{D}_B$ reaches its limit at a certain value of $\overline{U}_{GS}$ for $\overline{D}_N$ greater than about 0.1. This is because the inertia of a bubble increases with increasing $\overline{U}_{GS}$ and the superficial liquid velocity for high Re_P and low We_P is so low that the drag force of liquid is not enough to make the bubble detach even if $\overline{D}_B$ reaches its limit. The value of this $\overline{U}_{GS}$ increases with increasing We_P for a fixed Re_P and with decreasing Re_P for a fixed We_P. This means the relative

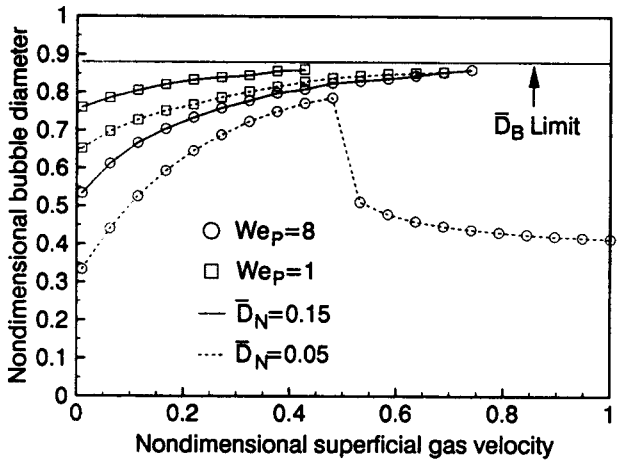

(a) Reference Reynolds number Re_P=1000

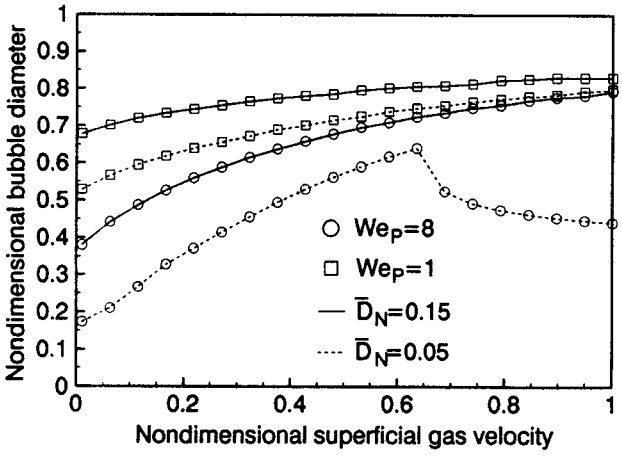

(b) Reference Reynolds number Re_P=400

Figure 6. Variation of nondimensional bubble diameter in air-water system in microgravity.

magnitude of liquid drag force to the surface tension force at the nozzle increases with decreasing Re_P and with increasing We_P. In the region of $\bar{U}_{GS}$, greater than this value, an elongated large Taylor bubble is expected to be formed. However, Figure 6b shows that $\bar{D}_B$ increases monotonically with $\bar{U}_{GS}$ without reaching its limit for all range of We_P and even for $\bar{D}_N$ greater than 0.1. For low Re_P, the superficial liquid velocity becomes high and the pipe diameter is so small that the liquid drag force compared to other forces becomes dominant and the bubble is swept away from the nozzle even in the region of high $\bar{U}_{GS}$. The effect of $\bar{D}_N$ on the bubble size decreases as $\bar{U}_{GS}$ increases because the relative magnitude of the surface tension force to the inertia of the bubble decreases as $\bar{U}_{GS}$ increases. If the nozzle diameter is less than 0.1 and We_P is high, Figures 6a and 6b show that $\bar{D}_B$ increases with increasing $\bar{U}_{GS}$ up to a certain value and then sharply decreases with further increase in $\bar{U}_{GS}$. This is due to the gas momentum flux in the region of high $\bar{U}_{GS}$. The gas momentum flux is inversely proportional to the square of $\bar{D}_N$ and the relative magnitude of that momentum to the surface tension force increases with increasing We_P. Thus, for small $\bar{D}_N$ and high We_P, momentum is enough to make the bubble detach even in the region of high $\bar{U}_{GS}$. In

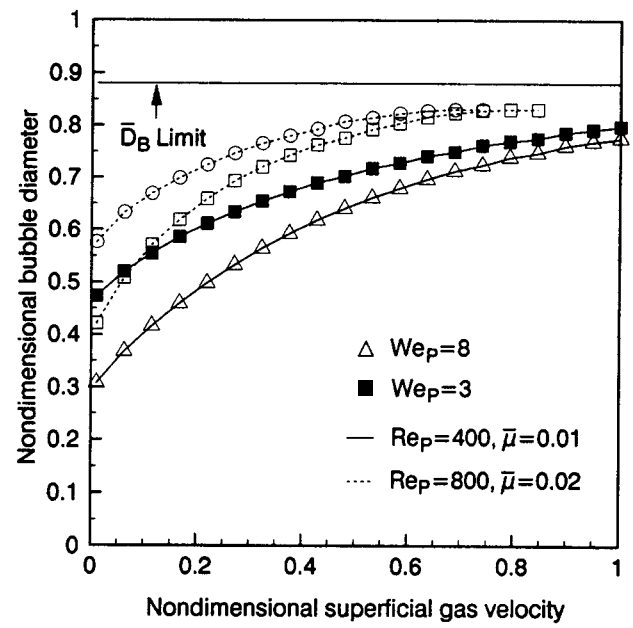

Figure 7. Variation of nondimensional bubble diameter for liquids of different viscosities in microgravity ($\bar{\rho}$ = 0.0012, $\bar{D}_N$ = 0.1).

this situation, the bubble detaches before it is swept away by the flowing liquid and the detachment condition of the bubble has been changed from Eqs. 16b to 16a, which is responsible for the discontinuities in Figure 6 and other figures. Similar discontinuities can be seen also in Figure 3. If We_P is low, this phenomena disappears regardless of the value of $\bar{D}_N$. This means the effect of the gas momentum flux in the range of low We_P is not great even if $\bar{D}_N$ is small and $\bar{U}_{GS}$ reaches its maximum value.

Figure 7 shows the effect of the liquid viscosity, μ_c, on the bubble size, in which the liquid viscosity of the dotted line is twice that of the solid line. For a fixed We_P, $\bar{D}_B$ for the more viscous liquid is smaller than that for the less viscous in the entire range of $\bar{U}_{GS}$, because the drag force of the liquid increases with increasing viscosity of the liquid. For the same variation of We_P from 3 to 8, the reduction of $\bar{D}_B$ is larger for the more viscous liquid than for the less viscous at any fixed $\bar{U}_{GS}$. This means the effect of the superficial liquid velocity on bubble size is greater for the more viscous liquid compared to that for the less viscous liquid. This result is believed to be due to the nonlinearity of the drag coefficient. For any fixed superficial liquid velocity, the Reynolds number of the more viscous liquid is lower than that for the less viscous and the variation of the drag coefficient is greater in the region of low Reynolds number than in the high region. The reduction of $\bar{D}_B$ decreases with increasing $\bar{U}_{GS}$ because the inertia of bubble increases with increasing $\bar{U}_{GS}$. Ghosh and Ulbrecht (1989) found that the size of a bubble formed in a shear flow decreased with increasing the superficial liquid velocity and the reduction of bubble size is greater for the more viscous liquid than that for the less viscous. Our results show the same trend.

Figure 8 shows the effect of the pipe diameter on the bubble size, in which the pipe diameter for the dotted line is twice that for the solid line and the nozzle diameter maintains con-

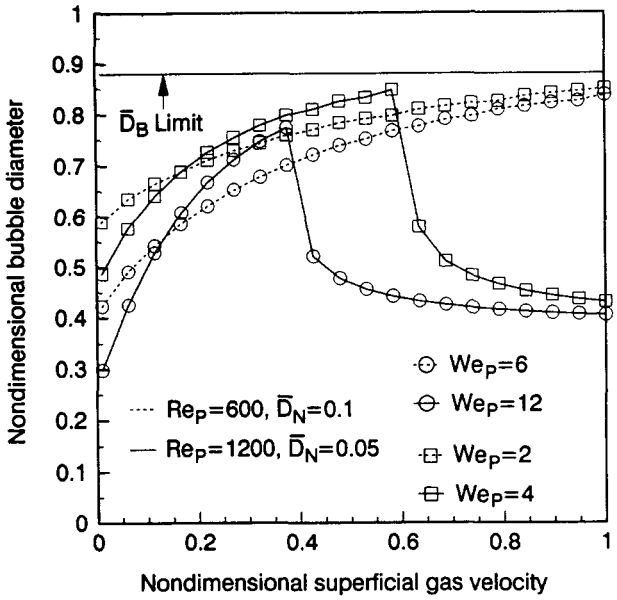

Figure 8. Variation of nondimensional bubble diameter for different pipe diameters in microgravity ($\bar{\rho} = 0.0012$, $\bar{\mu} = 0.02$).

stant. For a given We_P, $\bar{D}_B$, the bubble size for the pipe of larger diameter is smaller than that for the smaller diameter in the region of low $\bar{U}_{GS}$. This is because the bubble size is determined from the force balance between the surface tension force and the liquid drag force and the surface tension force for the pipe of smaller diameter is greater than that for the larger pipe diameter. Thus, the liquid drag force, which is necessary for the bubble detachment, should be larger for the smaller pipe than for the larger pipe. As $\bar{U}_{GS}$ increases, the difference between $\bar{D}_B$ of the two different pipe diameters decreases and that difference becomes zero at a certain value of $\bar{U}_{GS}$, and then further increases in $\bar{U}_{GS}$ reverses the situation,

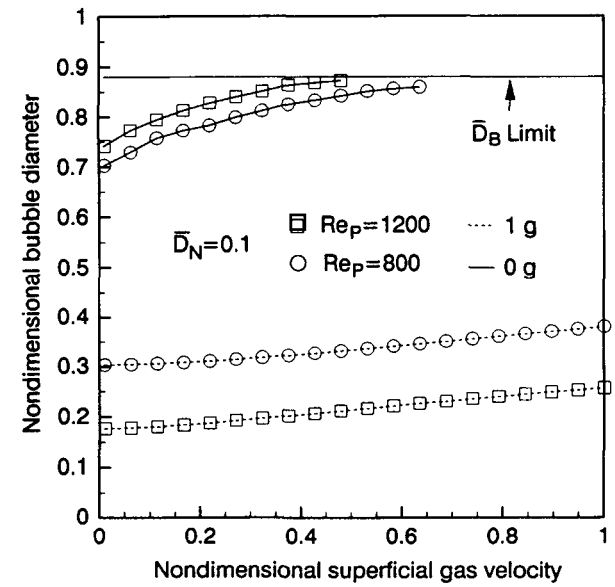

Figure 9. Difference in bubble size between normal gravity and microgravity ($We_P = 1$).

that is, $\bar{D}_B$ for the pipe of larger diameter is greater than that for the smaller pipe, and the difference between $\bar{D}_B$ for the two different pipe diameters increases as $\bar{U}_{GS}$ increases. This can be explained as follows. As $\bar{U}_{GS}$ increases, the inertia of bubble increases and the relative magnitude of the surface tension force at the nozzle decreases. Then, at a certain value of $\bar{U}_{GS}$, the magnitudes of $\bar{D}_B$ of the two different pipe diameters reach the same value. However, the wall effect at the same superficial liquid velocity is more significant for the pipe of smaller diameter than for the larger pipe. Thus, for the same size of $\bar{D}_B$, the relative magnitude of the drag force of the liquid to the inertia of the bubble is larger for the smaller pipe than for the larger pipe. Therefore, $\bar{D}_B$ for the larger pipe becomes greater than that for the smaller pipe beyond a critical value of $\bar{U}_{GS}$. This value of $\bar{U}_{GS}$, as well as the magnitude of $\bar{D}_B$ at this value of $\bar{U}_{GS}$, increases with decreasing superficial liquid velocity, because the relative magnitude of the surface tension force at the nozzle to the other forces likewise increases. For the larger pipe diameter, $\bar{D}_B$ increases with increasing $\bar{U}_{GS}$ up to a certain value, and then sharply decreases and asymptotically approaches a constant at large $\bar{U}_{GS}$. This is due to the gas momentum flux in the region of high $\bar{U}_{GS}$. In this situation, the bubble detaches before it is swept away by the flowing liquid and the detachment condition of the bubble has been changed from Eqs. 16b to 16a.

Figure 9 shows the difference in the bubble size of an air-water system between normal gravity and microgravity for low We_P. $\bar{D}_B$ in microgravity becomes nearly equal to the pipe diameter at a certain value of $\bar{U}_{GS}$, but the bubble size remains relatively small in normal gravity. Whereas the bubble detaches with the detachment condition of Eq. 16b in microgravity, the bubble detachment in normal gravity is determined by Eq. 16a. This is due to the fact that the bubble detachment depends only on the liquid drag force in microgravity, while the detachment in normal gravity depends both on buoyancy force and the liquid drag force. Thus, the major difference in the bubble size between normal and microgravity is expected in the region of low liquid velocity in which the liquid drag is much smaller than buoyancy in normal gravity. As the liquid velocity increases, the liquid drag force becomes dominant and the difference of the bubble size decreases.

Conclusion

A purely theoretical two-stage model for bubble and drop formation, applicable for terrestrial and microgravity environments, has been developed and the model was found to provide a satisfactory representation of the mechanism of a bubble formation process in flowing liquids. The predictions of the model are in good agreement with the experimental results in normal gravity. Based on the model, the bubble sizes are computed under various conditions in microgravity. In the region of low liquid velocity, the bubble becomes much larger than that in normal gravity. It is believed that the drag coefficient, as well as the effective cross-sectional area, are very important in the modeling, and more study of these parameters are necessary for a better predictive model formulation.

Acknowledgment

We gratefully acknowledge support from the National Aeronautics and Space Administration, Grant No. C-21066-G.

Notation

A_{eff} = effective cross-sectional area of bubble, cm^2
C_D = drag coefficient in infinite liquid
C_{DW} = drag coefficient in bounded liquid
C_M = added mass coefficients
D_B = bubble or drop diameter, cm
D_N = nozzle diameter, cm
D_P = pipe diameter, cm
F_B = buoyancy force, dyne
F_D = drag force, dyne
F_I = inertia of bubble, dyne
F_M = momentum flux of dispersed phase, dyne
F_R = reference force, dyne
F_S = surface tension force, dyne
F_σ = surface tension force per unit length, $dyne \cdot cm^{-1}$
Fr = reference Froude number
g = gravitational field, $cm \cdot s^{-2}$
l_B = travel distance of bubble, cm
L_N = length of bubble neck, cm
M = inertia mass of bubble, g
$\hat{n}$ = normal unit vector from surface of sphere
N = number of spheres
Q_c = flow rate of continuous phase, $cm^3 \cdot s^{-1}$
Q_d = flow rate of dispersed phase, $cm^3 \cdot s^{-1}$
Re_B = bubble Reynolds number
Re_P = reference Reynolds number
S = distance, cm
S = surface of bubbles
S_{ij} = surface of $(i, j)_{th}$ bubble
t = time, s
t_s = bubble formation time, s
T = total kinetic energy of liquid, dyne·cm
T_{ch} = kinetic energy of liquid within one channel, dyne·cm
U = uniform liquid velocity, $cm \cdot s^{-1}$
U_{eff} = effective velocity of continuous phase, $cm \cdot s^{-1}$
U_{GS} = superficial velocity of dispersed phase, $cm \cdot s^{-1}$
U_{LS} = superficial velocity of continuous phase, $cm \cdot s^{-1}$
U_S = superficial velocity of mixture, $cm \cdot s^{-1}$
U_T = terminal velocity in infinite liquid, $cm \cdot s^{-1}$
U_{TW} = terminal velocity in bounded liquid, $cm \cdot s^{-1}$
V = drop volume in flowing liquid, cm^3
V_O = Drop volume in quiescent liquid, cm^3
We_B = bubble Weber number
We_I = modified Weber number of Itoh (1980)
We_P = reference Weber number
X = position of bubble center in X direction, cm
Y = position of bubble center in Y direction, cm

Greek letters

ϵ = void fraction
η = contact angle of interface, radian
θ = azimuthal angle, radian
μ_c = viscosity of continuous phase, $dyne \cdot s \cdot cm^{-2}$
μ_d = viscosity of dispersed phase, $dyne \cdot s \cdot cm^{-2}$
$\bar{\mu}$ = viscosity ratio, μ_d/μ_c
ρ_c = density of continuous phase, $g \cdot cm^{-3}$
ρ_d = density of dispersed phase, $g \cdot cm^{-3}$
$\bar{\rho}$ = density ratio, ρ_d/ρ_c
σ = surface tension coefficient, $dyne \cdot cm^{-1}$
ϕ = angle of inclination, radian
Φ = velocity potential of liquid

Special symbols

- = nondimensional variable
→ = vector

Literature Cited

Al-Hayes, R. A. M., and R. H. S. Winterton, "Bubble Growth in Flowing Liquids," *Int. J. Heat Mass Transfer*, **24**, 213 (1981).

Al-Hayes, R. A. M., and R. H. S. Winterton, "Bubble Diameter on Detachment in Flowing Liquids," *Int. J. Heat Mass Transfer*, **24**, 223 (1981).

Bird, R. B., W. E. Stewart, and E. N. Lightfoot, *Transport Phenomena*, Wiley, New York (1960).

Chuang, S. C., and V. W. Goldschmidt, "Bubble Formation Due to a Submerged Capillary Tube in Quiescent and Coflowing Streams," *J. Basic Eng.*, **92**, 705 (1970).

Clift, R., J. R. Grace, and M. E. Weber, *Bubbles, Drops, and Particles*, Academic Press, New York (1978).

Currie, I. G., *Fundamental Mechanics of Fluids*, McGraw Hill, New York (1974).

Dukler, A. E., J. A. Fabre, J. B. McQuillen, and R. Vernon, "Gas-Liquid Flow at Microgravity Conditions; Flow Patterns and their Transitions," *Int. J. Multiphase Flow*, **14**, 389 (1988).

Eastman, R. E., C. J. Feldmanis, W. L. Haskin, K. L. Weaver, "Two-Phase Fluid Thermal Transport for Spacecraft," AFWAL-TR-84-3028 (1984).

Ghosh, A. K., and J. J. Ulbrecht, "Bubble Formation from a Sparger in Polymer Solutions: II. Moving Liquid," *Chem. Eng. Sci.*, **44**, 969 (1989).

Grace, J. R., T. Wairegi, and T. H. Nguyen, "Shapes and Velocities of Single Drops and Bubbles Moving Freely through Immiscible Liquids," *Trans. Instn. Chem. Engrs.*, **54**, 167 (1976).

Hadamard, J. S., "Mouvement Permanent lent d'une Sphere Liquide Visqueuse dans un Liquid Visqueux," *Compt. Rend. Acad. Sci.*, **152**, 1735 (1911).

Hamielec, A. E., and A. I. Johnson, "Viscous Flow around Fluid Spheres at Intermediate Reynolds Number," *Can. J. Chem. Eng.*, **40**, 41 (1962).

Itoh, R., Y. Hirata, K. Inoue, and Y. Kitagawa, "Formation of a Liquid Drop at a Single Nozzle in a Uniform Stream," *Int. Chem. Eng.*, **20**, 616 (1980).

Kawase, Y., and J. J. Ulbrecht, "Formation of Drops and Bubbles in Flowing Liquids," *Ind. Eng. Chem. Process Des. Dev.*, **20**, 636 (1981).

Kim, I., "Modeling of Bubble and Drop Formation in Flowing Liquids in Terrestrial and Microgravity Environments," PhD Thesis, Case Western Reserve Univ., Cleveland, OH (1992).

Kumar, R., and N. R. Kuloor, "The Formation of Bubbles and Drops," *Adv. Chem. Eng.*, **8**, 255, Academic Press, New York (1990).

Milne-Thompson, L. M., *Theoretical Hydrodynamics*, Macmillan, New York (1968).

Räbiger, N., and A. Vogelpohl, "Bubble Formation in Stagnant and Flowing Newtonian Liquids," *Ger. Chem. Eng.*, **5**, 314 (1982).

Räbiger, N., and A. Vogelpohl, "Calculation of Bubble Size in the Bubble and Jet Regimes for Stagnant and Flowing Newtonian Liquids," *Ger. Chem. Eng.*, **6**, 173 (1983).

Sada, E., A. Yasunishi, S. Katoh, and M. Nishioka, "Bubble Formation in Flowing Liquid," *Can. J. Chem. Eng.*, **56**, 669 (1978).

Sullivan, S. L., Jr., B. W. Hardy, and C. D. Holland, "Formation of Air Bubbles at Orifices Submerged Beneath Liquids," *AIChE J.*, **10**, 848 (1964).

Tsuge, H., S. Hibino, and U. Nojima, "Volume of a Bubble Formed at a Single Submerged Orifice in a Flowing Liquid," *Int. Chem. Eng.*, **21**, 630 (1981).

Tsuge, H., and S. Hibino, "Bubble Formation from an Orifice Submerged in Liquids," *Chem. Eng. Comm.*, **22**, 63 (1983).

Appendix

The kinetic energy of a fluid induced by the passage of a body through it is given by (Currie, 1974):

$$T = -\frac{1}{2}\rho_c \int_S \Phi \frac{\partial \Phi}{\partial \hat{n}}\, dS \qquad \text{(A1)}$$

where S is the surface of the moving body and Φ is the velocity potential. If there are confining walls for the fluid, the wall effect on the fluid motion can be taken into account by the method of images in which the mirror images of the body are placed to simulate the walls (Milne-Thompson, 1968). Since the method is applicable to straight walls, the flow in a pipe

in the present problem is approximated by that through a square channel with the same cross-sectional area as the pipe. Then, the kinetic energy of the flow within the channel due to a moving sphere can be obtained by considering an infinite array of spheres of the same size moving with the same velocity in an infinite medium.

In the present problem, the bubble moves in both X and Y directions, so we need to compute the added mass coefficient for a sphere moving normal or parallel to the channel. The procedure to obtain the velocity potentials for those two cases is very lengthy. It is described in detail in Kim et al. (1992), so only the major results are given herein.

In the case of a sphere moving parallel to the channel, the kinetic energy of the fluid within the square channel of side length L_c is given by:

$$T_{ch}=\frac{1}{2}\left[\frac{1}{2}+\frac{3}{2}\left(\frac{R}{L_c}\right)^3+\frac{3}{2}\frac{R^3}{(L_c^2+H^2)^{3/2}}+\frac{3}{4}\left(\frac{R}{H}\right)^3 +\frac{3}{4}\frac{R^3}{(2L_c-H)^3}+\frac{3}{2}\frac{R^3}{\{(2L_c-H)^2+L_c^2\}^{2/3}}\right]M_SU^2 \quad \text{(A2)}$$

where $M_S=(\psi/3)\rho_c\pi R^3$ in the mass of the fluid replaced by the sphere, R the sphere radius, H the distance to the sphere center from the channel bottom, and U the speed of the sphere. Then, the added mass coefficient is obtained as $C_{MX}=T_{ch}/(1/2)\,M_SU^2$ by definition.

For a sphere moving normal to the channel the kinetic energy in the channel is:

$$T_{ch}=\frac{1}{2}\left[\frac{1}{2}+\frac{3}{2}\left(\frac{R}{H}\right)^3+\frac{3}{2}\left(\frac{R}{2L_c-H}\right)^3+\frac{3}{2}\left(\frac{R}{L_c}\right)^3 +\frac{1}{2}\frac{R^3(L_c+6H)}{(L_c^2+H^2)^2}+\frac{1}{2}\frac{R^3(11L_c-6H)}{\{(2L_c-H)^2+L_c^2\}}\right]M_SU^2 \quad \text{(A3)}$$

and then the added mass coefficient is $C_{MY}=T_{ch}/(1/2)M_SU^2$.

Manuscript received May 18, 1992, and revision received May 3, 1993.